Plasma Sources Sci. Technol. 3 (1994) 162–168. Printed in the UK

RF compensated probes for high-density discharges

Isaac D Sudit and Francis F Chen

Electrical Engineering Department, University of California, Los Angeles, California 90024-1594, USA

Received 2 September 1993, in final form 29 November 1993

Abstract. A Langmuir probe for the study of high-density RF discharges has been developed and tested in a helicon discharge in which the RF potential (≈ 100 V) is much larger than the electron temperature (≈ 4 eV). Carbon probe tips are used to minimize erosion by ion sputtering. Miniature RF chokes located close to the probe tip present RF impedances of 150 kΩ at the operating frequency of 27.12 MHz and 300 kΩ at the first harmonic at 54.24 MHz. It is further necessary to drive the probe tip to follow the RF fluctuations by coupling it to a larger floating electrode. We have been able to measure T_e values as low as 3.4 eV in argon plasmas of 10^{13} cm^{-3} density; these temperatures are 1.6 eV lower than ones measured by probes with chokes alone, and 2.3 eV lower than measured by uncompensated probes.

1. Introduction

Inductive coupling of helicon waves has been shown to be a very efficient source of plasma production [1, 2]. The high densities (10^{13} cm^{-3}) obtained at low neutral pressures (a few mTorr) has sparked interest in the use of this technology for plasma etching [3, 4]. As is the case with all plasma sources used in etching, a low electron temperature is desirable in order to improve anisotropy, i.e. reduce ion temperature, as well as to minimize wafer damage. It is therefore important to be able to measure the electron temperature accurately in such discharges. Knowledge of the electron temperature (and, in particular, of the electron energy distribution function (EEDF)) is also required to understand the ionization and excitation mechanisms of the discharge and to find the operating conditions that optimize its performance.

The effect of an oscillating plasma potential on Langmuir probes has long been recognized as a major difficulty in the interpretation of probe data [5, 6]. Boschi and Magistrelli [6] have shown that a sinusoidal time-varying plasma potential has the effect of distorting the electron retardation region of the probe trace and of shifting the floating potential towards more negative voltages. It is well known that in Maxwellian plasmas the average electron current in the presence of periodic potential fluctuations still gives the correct temperature as long as the current does not leave the exponential region. However, if the RF excursions bring the electron current out of the exponential region, the usual graphical methods of analysing electron currents overestimate the electron temperature.

A DC probe trace would be obtained in such plasmas if the probes were allowed to follow the plasma potential oscillations. Many authors have tried several methods to accomplish this. Chen [7] measured the instantaneous current and floating potential with a double probe and displayed them on the y and x axes of an oscilloscope without averaging. This method had a frequency response below 1 MHz. Cantin and Gagne [8] fed the RF voltage of a floating electrode to a probe in a 3.5 MHz argon discharge through a unity gain amplifier and used resonant inductors to increase the circuit impedance. The major disadvantage of their method is the limitation of the amplifier to RF voltages of only 9 V peak-to-peak. Braithwaite *et al* [9] applied the attenuated and phase shifted voltage of the powered electrode in a 13.56 MHz parallel plate discharge to a Langmuir probe. The amplitude and phase of the signal were varied until the most positive floating potential was obtained. This method does not allow for the presence of higher harmonics in the plasma. Paranjpe *et al* [10] and Lai *et al* [11] have both used a copper rod inside a glass holder in series with a Langmuir probe to increase the coupling of the probe to the plasma potential fluctuations. The large rod required to implement this method in our small diameter discharge would significantly disturb the plasma.

In this paper we describe a probe designed to work in a 27.12 MHz helicon discharge. The RF compensation method is similar to the one adapted by Godyak *et al* [12] to RIE (reactive ion etching) discharges. However, the environment is quite different for a probe in a helicon source than in an RIE discharge. The strong magnetic field causes the logarithm of the electron current to deviate from linearity at potentials well below the space potential, so that RF compensation needs to be more accurate. The magnetic field also does not tolerate obstacles much larger than the electron Larmor radius,

0963-0252/94/020162 + 07 $19.50

which can deplete the electrons in the blocked tube of force. The harmonic content of the fluctuations can also be different. There are small populations of fast electrons, which may be hard to detect. On the other hand, there are no violent sheath motions and plasma flows, such as occur in RIE discharges, which may bring the probe into the sheath region.

In our method, a floating electrode exposed to the plasma is coupled to a cylindrical Langmuir probe through a large (4.1 nF) capacitor. The electrode is placed as near the probe tip as possible so as to sample the local fluctuating plasma potential without any additional disturbance to the plasma. Miniature RF chokes with impedances larger than 100 kΩ at the first two harmonics are connected near the probe tip. Electron temperatures as low as 3.4 eV have been measured in $10^{13}\,cm^{-3}$ plasmas at 1.6 kW RF power, and 2.3 eV at 400 W. Probes without the floating electrode and probes with no compensation at all both overestimate the temperature, the latter by the larger factor. The material of the probe holder is not important as long as the chokes are placed near the probe tip. The results also show the importance of second harmonic compensation.

2. Probe design

2.1. Circuit design

Figure 1 shows the equivalent circuit of the probe, sheath, and associated circuitry. Here V_s is the space or plasma potential, V_p the potential of the probe tip, V_b the probe bias voltage, and V_0 the output voltage across the current measuring resistor R_m (1 kΩ here). The sheath impedance Z_{sh} consists of an equivalent resistance R_{sh} in parallel with an equivalent capacitance C_{sh}. The series of chokes is represented by an impedance Z_{ck}. The small stray capacitance C_{s1} is that of the short lead between the chokes and the probe tip and large stray capacitance C_{s2} is that of the power supply and all the connecting cables. The auxiliary floating electrode has an impedance Z_x consisting of R_x in parallel with C_x, and is coupled to the probe tip by the coupling capacitor C_{cp} mentioned above. The space potential is given by

$$V_s = V_{DC} + V_{RF} \tag{1}$$

where V_{RF} is the RF oscillation about the mean value V_{DC}.

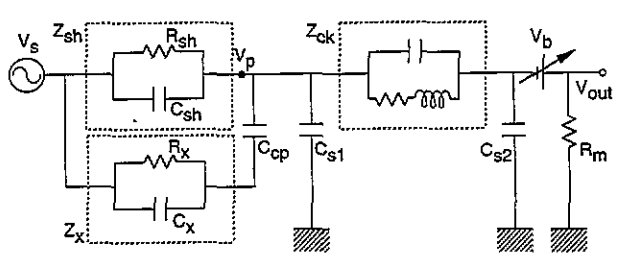

Figure 1. Equivalent circuit for the probe, sheath, and measurement system.

2.1.1. DC signals. When V_{RF} is zero, the DC current to the probe, which is the quantity we wish to measure, is given by

$$I = I_i - I_e$$

where

$$I_e = neA_p v_e e^{e(V_p - V_s)/kT_e} \tag{2}$$

$$I_i \approx \tfrac{1}{2} neA_p v_s \tag{3}$$

$$v_e = (kT_e/2\pi m)^{1/2} \tag{4}$$

$$v_s \approx (kT_e/M)^{1/2} \tag{5}$$

with $V_s = V_{DC}$. The probe potential V_p is equal to the floating potential V_f when I_i is equal to I_e; this gives

$$V_f = V_s - \frac{kT_e}{2e}\ln\left(\frac{2M}{\pi m}\right). \tag{6}$$

The effective sheath resistance is given by

$$\frac{1}{R_{sh}} = \frac{dI}{dV} \approx -\frac{dI_e}{dV}. \tag{7}$$

Equation (2) then gives

$$R_{sh} = \frac{kT_e}{eI_e}. \tag{8}$$

This varies with $V_p - V_s$ since I_e does, but at the floating potential it has the unique value

$$R_{sh} = \frac{kT_e}{eI_i} \approx \frac{2\lambda_D^2}{\varepsilon_0 A_p v_s}. \tag{9}$$

The last relation comes from Equation (3) and the definition of Debye length

$$\lambda_D^2 = \varepsilon_0 kT_e/ne^2.$$

2.1.2. RF signals. We now let $V_s = V_{DC} + V_{RF}$, where $|V_{RF}|$ may be much larger than $|V_{DC}|$ with respect to ground. First, we neglect the compensation circuitry represented by Z_x and Z_{ck} so that V_p will be constant at V_b and $V_p - V_s$ will oscillate wildly. Since I_e oscillates, R_{sh} will also change during the RF cycle. In addition, an RF current will now flow through the capacitance C_{sh}, which we now calculate.

The dynamic sheath capacitance can be defined by

$$C_{sh} = \frac{\Delta Q}{\Delta V} \tag{10}$$

where $V = V_p - V_s$ and Q is the charge on either side of the capacitor. Since measurements are made near the floating potential because the I–V curve is distorted by the magnetic field elsewhere, the probe will nearly always be sufficiently negative with respect to the plasma that a Child–Langmuir sheath forms adjacent to the probe surface. We can therefore calculate ΔQ from the surface charge on the probe. The other side of the capacitor is the transition to the Debye sheath (the transition to the quasi-neutral region) and is not well defined. This approximation fails if the RF fluctuations bring V_s so close to V_f that the Debye sheath extends to

the probe. We also neglect the potential drop in the Debye sheath compared with the total sheath drop. Implicit in this approach is the assumption that the sheath comes to equilibrium at each phase on the RF cycle. This assumption is justified if the RF frequency is much smaller than the ion plasma frequency [13]. The physical reason for this is that the sheath can adjust itself on the timescale for an ion to traverse the sheath. Since the sheath has dimensions of order $2\pi\lambda_D$ while the ions have velocities of order v_s, this time is of the order $2\pi\lambda_D/v_s$, which is just $1/f_{pi}$. For $n = 10^{13}\,\mathrm{cm}^{-3}$, f_{pi} is of the order of 100 MHz for argon, so that this condition is barely met at 27 MHz. At lower densities, this condition can still be met at 13.56 MHz with a lower ion mass. At frequencies above 27.12 MHz and lower densities, higher harmonics can be generated by the oscillating ion motion, an effect neglected here. Assuming a thin sheath so that planar geometry holds, we have from equation (10)

$$\frac{C_{sh}}{A_p} = \frac{\Delta\rho_s}{\Delta V} = \varepsilon_0 \frac{\Delta E}{\Delta V} = -\varepsilon_0 \frac{\mathrm{d}}{\mathrm{d}V}\left(\frac{\mathrm{d}V}{\mathrm{d}x}\right) \tag{11}$$

where $V = V_p - V_s$ and the boundary condition on the probe surface gives the surface charge ρ_s. The right-hand side of equation (11) can be evaluated from the Child–Langmuir formula, modified by the incident ion velocity v_s, which can be derived as follows.

Energy conservation for the ion gives

$$W_0 \equiv \tfrac{1}{2}Mv_s^2 = \tfrac{1}{2}Mv^2 + eV \qquad (V<0) \tag{12}$$

while continuity of ion flux and Poisson's equation give

$$n_s v_s \approx \frac{n_0}{2} v_s = nv \tag{13}$$

$$\varepsilon_0 \frac{\mathrm{d}^2V}{\mathrm{d}x^2} = -en. \tag{14}$$

Combining these, we obtain

$$\frac{\mathrm{d}V}{\mathrm{d}x}\frac{\mathrm{d}^2V}{\mathrm{d}x^2} = -\frac{en_0}{2\varepsilon_0}\left(1-\frac{eV}{W_0}\right)^{-1/2}\frac{\mathrm{d}V}{\mathrm{d}x}. \tag{15}$$

The first integral yields $(\mathrm{d}V/\mathrm{d}x)^2$, and the appropriate root is

$$\frac{\mathrm{d}V}{\mathrm{d}x} = -2\left(\frac{n_0W_0}{2\varepsilon_0}\right)^{1/2}\left[\left(1-\frac{eV}{W_0}\right)^{1/2}-1\right]^{1/2}. \tag{16}$$

Taking the derivative with respect to V and inserting into equation (11), we obtain, for $|W_0/eV| \ll 1$

$$\frac{C_{sh}}{A_p} = \frac{e}{2}\left(\frac{n_0\varepsilon_0}{2W_0}\right)^{1/2}\left(-\frac{eV}{W_0}\right)^{-3/4}\left[1+\frac{1}{2}\left(\frac{W_0}{-eV}\right)^{1/2}\right]. \tag{17}$$

In terms of the incident ion current density

$$J = \frac{n_0}{2}ev_s = \frac{n_0e}{2}\left(\frac{2W_0}{M}\right)^{1/2} \tag{18}$$

this is

$$\frac{C_{sh}}{A_p} = \frac{1}{2}\left(\frac{M}{2e}\right)^{1/4}(\varepsilon_0 J)^{1/2}(-V)^{-3/4}\left[1+\frac{1}{2}\left(\frac{W_0}{-eV}\right)^{1/2}\right] \tag{19}$$

in which the W_0 correction term is usually small. As V_s oscillates with RF, the sheath capacitance changes, so harmonics in the probe current will be generated even if V_{RF} is sinusoidal.

The magnitude of the second harmonic can be estimated as follows. Let $V_s = V_{DC} + V_{RF}\sin\omega t$. Then V in equation (19) is given by

$$V = V_p - V_s = V_p - V_{DC} - V_{RF}\sin\omega t. \tag{20}$$

The capacitance C_0 in the absence of V_{RF} is

$$\frac{C_0}{A_p} = \frac{1}{2}\left(\frac{M}{2e}\right)^{1/4}(\varepsilon_0 J)^{1/2}(V_{DC}-V_p)^{-3/4} \tag{21}$$

which, together with equation (5) and (18), takes the simple form

$$C_0 = \frac{\varepsilon_0 A_p}{2^{7/4}\lambda_D}\left[\frac{e(V_{DC}-V_p)}{kT_e}\right]^{-3/4}. \tag{22}$$

The instantaneous capacitance is then given by

$$\frac{C_{sh}}{C_0} = \left(1+\frac{V_{RF}\sin\omega t}{V_{DC}-V_p}\right)^{-3/4}. \tag{23}$$

The current $i = C(\mathrm{d}V/\mathrm{d}t)$ into the probe is then

$$i = C_0\left(1+\frac{V_{RF}\sin\omega t}{V_{DC}-V_p}\right)^{-3/4}(-V_{RF}\omega\cos\omega t) \tag{24}$$

The second harmonic at 2ω is experimentally found to be dominant. This can be found by expanding the $-3/4$ power in a Taylor series:

$$i = C_0\left(1-\frac{3}{4}\frac{V_{RF}\sin\omega t}{V_{DC}-V_p}\right)(-V_{RF}\omega\cos\omega t). \tag{25}$$

This current will give rise to voltages at ω and 2ω across the resistor R_m, and the relative magnitude of the harmonic to the fundamental is

$$\frac{C_1}{C_0} = \frac{3}{8}\left|\frac{V_{RF}}{V_{DC}-V_p}\right|. \tag{26}$$

Normally, this is so large that the expansion is invalid; but with proper RF compensation, V_p follows the oscillations V_{RF}, so that V in equation (20) is constant, and therefore C_{sh} does not fluctuate, and there are no harmonics at all unless they exist in V_{RF}.

2.1.3. RF-compensation. To avoid the large swings in $V_s - V_p$, it is customary to add resonant inductors near the probe tip which can present a large impedance to the RF signals but not to low-frequency signals. Since V_{RF} can contain a large second harmonic, these chokes have to resonate at both ω and 2ω. Since the chokes must be placed in the probe shaft, it is critical to find chokes that are small enough to fit but still have a large enough Q to give the required impedance. Neglecting for now the

auxiliary electrode Z_x and the stray capacitance C_{s1} in figure 1, we see that Z_{sh} and Z_{ck} form a voltage divider such that

$$V_p = \frac{Z_{ck}}{Z_{sh} + Z_{ck}} V_s. \tag{27}$$

Since $V_p - V_s$ must be held, in the presence of large V_{RF} swings, to much less than kT_e/e in order to resolve features in the $I-V$ characteristics and to prevent excursions into the electron saturation region, we require

$$\frac{Z_{ck}}{Z_{sh} + Z_{ck}} |V_{RF}| \ll \frac{kT_e}{e} \tag{28}$$

or

$$Z_{ck} \gg Z_{sh}\left(\frac{e|V_{RF}|}{kT_e} - 1\right). \tag{29}$$

It is unavoidable to have at least 1 pF of stray capacitance C_{s1} to ground of the lead from the chokes to the probe tip, and of the chokes themselves. The impedance $Z_{s1} = 1/j\omega C_{s1}$ must also satisfy equation (29), so that Z_{ck} in (29) should be interpreted as the parallel combination of Z_{ck} and Z_{s1}. For large RF potentials, it is generally not possible to satisfy this condition, but one can add an auxiliary electrode as close as possible to the probe tip. This electrode should have an area A_x much larger than the probe area A_p and be coupled to the probe tip through a capacitor C_{cp} which is so large that it is a short circuit for RF signals but small enough that it does not pass low-frequency signals. In that case, the probe tip will be driven to follow the RF fluctuations through an impedance Z_x that is identical to Z_{sh} (both real and imaginary parts) but much smaller in magnitude. The dominant impedances must therefore satisfy

$$Z_c \gg Z_x\left(\frac{e|V_{RF}|}{kT_e} - 1\right) \tag{30}$$

where Z_c is the smaller of Z_{ck} and Z_{s1}.

2.1.4. Low-frequency signals. Real oscillations in plasma density and potential may occur in the 1–1000 kHz regime because of instabilities and other effects in the discharge. These oscillations can be seen by proper design of the chokes and the coupling capacitor so that Z_{ck} is effectively zero and Z_x effectively infinite for these signals. A density fluctuation will manifest itself as a modulation of R_{sh} (equation (8)) because of the variation of the n factor in I_e (equation (2)). A low-frequency fluctuation in V_s will also modify I_e through the exponential factor in equation (2). The coupling of these signals through C_{sh} and C_{cp} should be negligible. However, these signals will not appear across the measuring resistor R_m if the stray capacitance C_{s2} is so large that $1/R_mC_{s2}$ is smaller than the low frequency being observed as is usually the case if V_b is supplied by an electronic power supply. To measure low-frequency fluctuations, one normally needs to take pains to minimize C_{s2} either by floating R_m above V_b and optically coupling the signal out, or by using for V_b batteries mounted away from the walls of the RF shields. When large values of R_m are used to measure floating potential fluctuations, C_{s2} consists of the cable capacitance, since no power supply is needed. In that case, capacitance neutralization may be necessary to make R_mC_{s2} sufficiently small.

2.1.5. Design Values. In the following computations, we assume a frequency of 27.12 MHz, a probe tip 0.3 mm in diameter and 1.5 mm long, and an argon plasma with $kT_e = 4$ eV and $n = 10^{13}\,\mathrm{cm}^{-3}$. These values give $\omega = 1.7\times10^8$, $A_p = 1.4\times10^{-6}\,\mathrm{m}^2$, $v_s = 3.1\times10^3\,\mathrm{m\,s}^{-1}$, and $I_i = 3.47$ mA. Equation (6) then gives $V_s - V_f = 5.35\,kT_e/e = 21.5$ V, while equation (9) gives $R_{sh} = 1.2\,k\Omega$ and equation (22) gives $C_0 = 0.22$ pF ($Z_{c0} = 26.7\,k\Omega$) at the floating potential. Thus $|Z_{sh}| \simeq 1\,k\Omega$. Though R_{sh} is smaller than Z_{c0} here, this will not be true at all densities. Since $Z_{c0} \propto n^{-1/2}$ while $R_{sh} \propto n^{-1}$, R_{sh} will dominate at $n < 2\times10^{10}\,\mathrm{cm}^{-3}$. If $|V_{RF}| \simeq 200$ V while $T_e \simeq 4$ eV, equation (29) requires that Z_{ck} be much larger than 50 kΩ, or of the order of 500 kΩ. This is impractical, 125 kΩ being the largest value consistently obtainable. Moreover, this impedance is shorted out by the stray capacitance C_{s1}, unless the latter is much less than 0.5 pF. For a realistic value of 1 pF, Z_{cs1} is of order 6 kΩ, which does not satisfy equation (29) except with small voltages V_{RF}. It is therefore necessary to add an auxiliary electrode with impedance Z_x. If, for instance the area A_x of this electrode is 50 times larger than A_p, the impedance Z_x will be 50 times smaller than Z_{sh}, or about 20 Ω. (As in the case of the probe, the electrode's Z_{cx} value is larger than R_x.) Using $Z_x = 20\,\Omega$, we see from equation (30) that adequate compensation is obtained for $|V_{RF}| \leqslant 1.2$ kV if $Z_c \simeq Z_{cs1} = 6\,k\Omega$ and for $|V_{RF}| \leqslant 25$ kV if $Z_c \simeq Z_{ck} = 125\,k\Omega$. Finally, we consider the coupling capacitor C_{cp} which should be much larger than C_x. If $C_x = 50\,C_{sh} \simeq 11$ pF, we may take C_{cp} to about 1 nF.

2.2. The helicon discharge

Figure 2 shows a schema of the discharge in which the experiments were conducted. The plasma is confined in a 1.6 m long, 5 cm diameter quartz tube, surrounded by 12 magnetic field coils, which provide a maximum uniform axial field of 0.13 T. There are three sets of three ports for diagnostics and gas feed as shown. The power is provided by a 2 kW Henry Radio amplifier operating at 27.12 MHz and coupled to the plasma through a 12 cm long, half-wavelength right helical antenna [2]. Power matching is achieved with a double-stub tuner made of 1.2 cm diameter rigid coaxial cable. The neutral gas is fed into the tube through one of the ports located at the centre of the tube and its pressure monitored with a Convectron® gauge located at the end of the discharge. Typical operating conditions had argon pressures between 7.5 and 10 mTorr, transmitted powers of about 1.5 kW, reflected powers of less than 40 W, and magnetic fields of $\simeq 0.08$ T. Both the magnetic field and

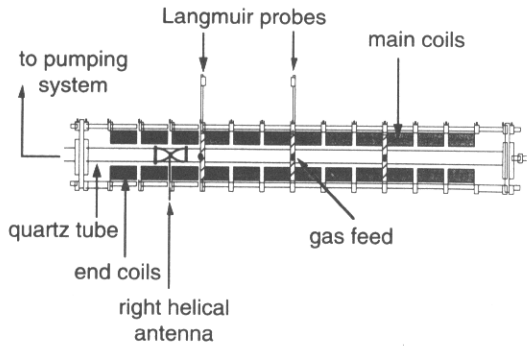

Figure 2. Schematic diagram of the apparatus.

the RF power were pulsed for approximately 50 ms, with about 2% duty cycle.

2.3. Probe design

Diagrams of the probe designed to work in the helicon discharge are shown in figure 3. The probe tip is made of 0.3 mm diameter graphite and has a length of 1.5 mm. It is glued with conducting epoxy adhesive inside a 0.74 mm OD hypodermic needle. The needle is inserted in a 1.6 mm OD ceramic tube, with the graphite not touching the inside the walls for at least 3 mm from the end of the ceramic. Tungsten wire 0.127 mm in diameter is closely wound 20 times around the ceramic tubing, starting at the probe tip end. The wire is run through a separate ceramic tube and electrically connected to the hypodermic needle through a 4.1 nF capacitor. The capacitor, as well as four miniature RF chokes in series with it, are located as close as physically possible to the needle, inside the main body of the probe holder, which consists of a 15 cm long, 6.35 mm OD glass tube. The last choke is followed by miniature coaxial cable which goes to the electronics. The effective area of the auxiliary electrode (half the area of the tungsten wire, or the part exposed to the plasma) is about 14 times the probe area.

The RF chokes are Lenox–Fungle subminiature shielded inductors. These inductors have 10% inductance tolerance and an unavoidable parallel capacitance which determines the resonant frequency. The DC resistance is about 2 Ω. Impedance–frequency curves have to be measured for each inductor individually before selection. The impedance–frequency curve for the chain of four inductors used is presented in figure 4. The impedance is 146 kΩ at 27 MHz and 296 kΩ at 54 MHz.

We have measured the oscillating RF plasma potential with a calibrated capacitive probe. The signals at ω and 2ω are strongest and of the order of 100 V peak-to-peak. The probe design satisfies the conditions for cancellation of these signals according to the preceding discussion. Neglecting the effect of C_{s1}, which cannot be measured, we estimate that the ratio of sheath impedance to circuit impedance is 5×10^{-4} and 2×10^{-4} at 27 MHz and 54 MHz respectively. At these densities and RF fluctuation levels, we should be able to resolve temperatures of approximately 0.05 eV. The stray capacitance C_{s1} would reduce the effectiveness of the chokes. Even if we assume that $Z_c \simeq Z_{cs1} = 6\,\text{k}\Omega$, we should be able to resolve temperatures as low as 1 eV. The probe voltage is supplied by a floating ± 100 V sweeper, which is floated above ground with a variable ± 100 V power supply. The probe current is measured as a voltage drop across a 1 kΩ resistor, and the probe voltage is measured between the probe and ground. The current–voltage trace is monitored and signal averaged on a digital oscilloscope and then transferred to a personal computer for data analysis. The sweeping time in these experiments was approximately 20 ms. The probe is swept during the second half of the RF pulse, which ensures that the discharge sampled is stable.

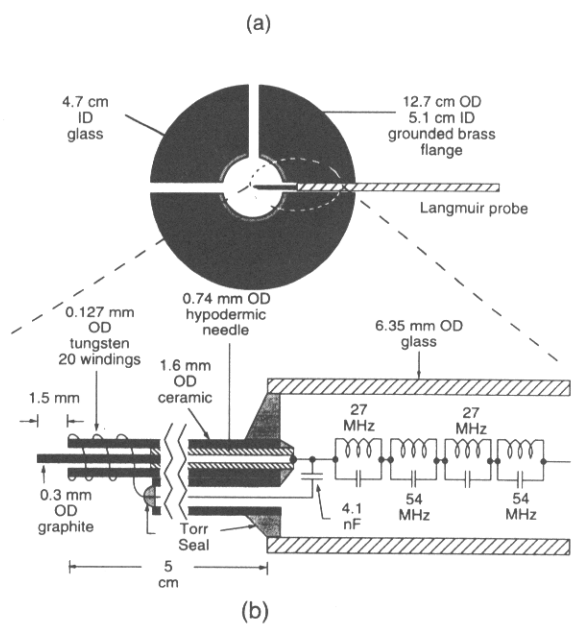

Figure 3. Mechanical design of the probe: (*a*) the entire probe drawn to scale, and (*b*) details of the probe tip area.

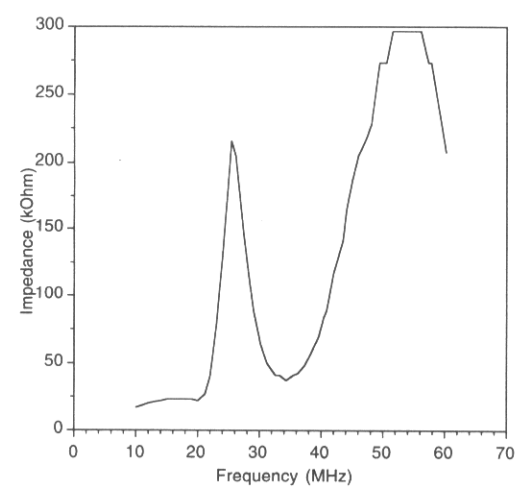

Figure 4. Impedance against frequency curve of four RF chokes in series used to increase the probe circuit impedance to ground.

3. Results

Strong magnetic fields can significantly affect the current–voltage characteristics of Langmuir probes. Sanmartin [14] and Stangeby [15] have studied probe current collection in dense ($\lambda_D \ll r_p$) magnetized plasmas. They have shown that the electron current is reduced by the field, and it departs from the characteristic exponential behaviour in the retardation region of the trace. This effect is more pronounced with increasing ratio of probe dimensions to Larmor radius. Only for very negative voltages, corresponding to electrons with a large Larmor radius, can the current be expected to increase exponentially with increasing bias voltage. We have therefore analysed the section of probe traces near the floating potential only.

In order to extend the electron current data available, it is necessary to subtract the ion contribution to the total probe current. We have found that the square of the ion current is proportional to the probe voltage, as expected in the high-density regime [16]. We have made linear fits to the square of the ion current and used them as baselines to obtain pure electron current. Figure 5 is a plot of the electron current to three Langmuir probes. Probe 1 has no RF compensation: it is constructed as described above, but it has neither chokes nor a floating electrode. Probe 2 has four chokes providing an impedance of 91 kΩ at 27 MHz and 198 kΩ at 54 MHz, but no floating electrode. Probe 3 has the full compensation circuitry described above. All probes have holders made of glass and were inserted to the centre of the discharge, one at a time. Each occupies one of the insertion ports shown in figure 2. The effect of the RF is obvious. As the RF compensation increases, the probe traces shift towards more positive voltage values. The curvature of the electron retardation region decreases as well. The lines on the figure correspond to exponential fits to the most negative linear regions in the logarithmic scale. As long as the fits are confined to this region, they agreed well with one another and all give electron temperatures of the order of 4 eV. As the RF compensation is increased, the range for which the currents fit an exponential function of the probe voltage increases. If we force an exponential fit to the entire electron current range up to 20 mA for each probe, as shown in figure 6, the temperatures, as well as the floating potentials, depend on the degree of RF compensation. We see that the probe without chokes overestimates kT_e by 1.8 eV, while the probe with only chokes overestimates by 1.1 eV.

Figures 7 and 8 demonstrate the importance of second harmonic compensation. Two probes with chokes that provide similar impedance for the first harmonic (100 kΩ and 88 kΩ) but impedances that are different by a factor of 15(193 kΩ and 12 kΩ) for the second harmonic have been used to measure kT_e. Figure

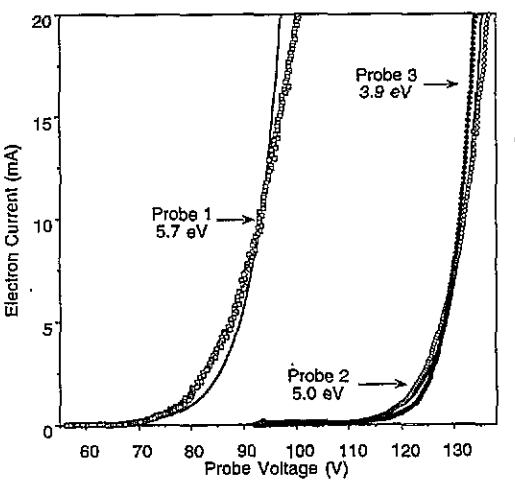

Figure 6. Exponential fits to electron currents collected by the three probes described in figure 5. The curves shown are the best fit over the entire current range, which is the same for all probes.

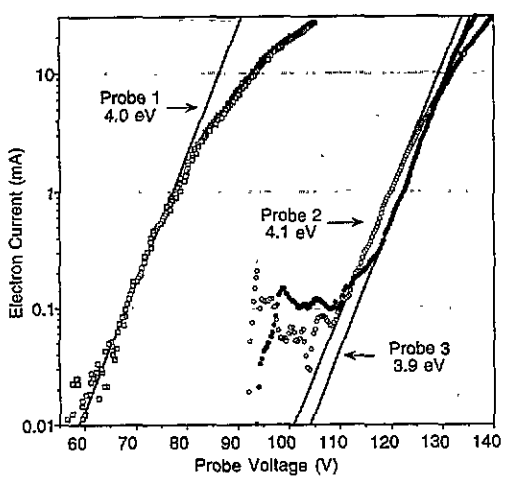

Figure 5. Semi-logarithmic plots of electron currents collected by three different probes in a 7.5 mTorr, 1.5 kW, 27.12 MHz helicon discharge in argon. Probe 1 has no RF compensation; probe 2 has RF chokes; probe 3 has RF chokes plus an auxiliary floating electrode, as shown in figure 4.

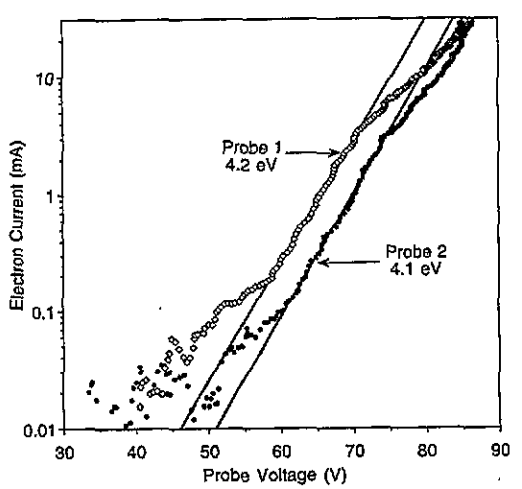

Figure 7. Electron I–V characteristic, as in figure 5, for two probes with different chokes. Probe 1 has large impedances for ω, while probe 2 has a large impedance for both ω and 2ω.

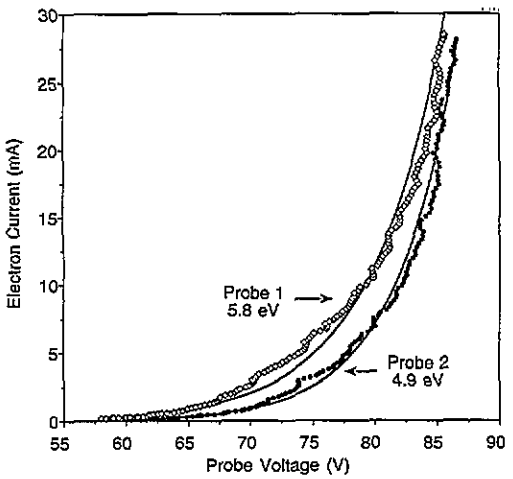

Figure 8. Electron I–V characteristics, as in figure 6, for the two probes described in figure 7.

7 shows currents collected by these probes in a logarithmic scale. The probe with strong second harmonic compensation (probe 2) yields a trace that is shifted towards more positive voltages. Exponential fits to the linear sections yield similar temperatures ($\sim$4 eV) for both probes. However, when the fits are made over equal current ranges, as shown in figure 8, the probe with weak second harmonic impedance (probe 1) overestimates the electron temperature by 0.9 eV.

The effect of different probe holder materials is shown in figure 9. Two probes are compared: probes 1 and 2 have both chokes and floating electrodes but have probe shafts made of glass and grounded stainless steel respectively. The material of the probe holder seems to have little effect on the accuracy of the temperature determination. The reason for this might be that both holders fit snugly inside grounded brass flanges, which provide a capacitance to ground even for the chokes in a glass shaft. If the RF compensation is adequate to cancel the effect of C_{s1} in the worst case, then the shaft material will not be important.

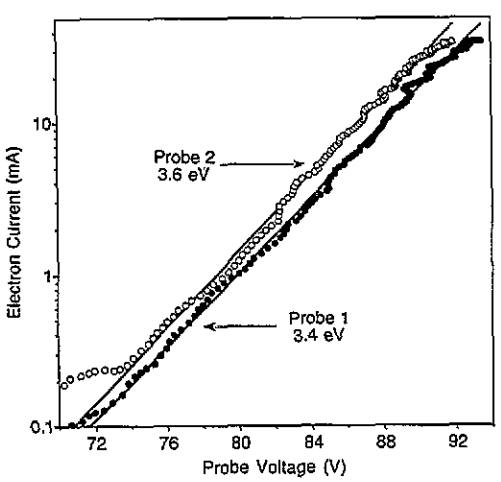

Figure 9. Electron I–V characteristics, as in figure 5, for two probes with full RF compensation. Probe 1 is mounted in a glass shaft, and probe 2 in a stainless steel shaft.

4. Conclusions

The probe design used in these experiments has allowed us to measure electron temperatures of about 4 eV, which are comparable to the temperatures found in other RF discharges used for plasma processing. The floating electrode incorporated in the design has the advantage of reducing the sheath impedance by coupling to the oscillating plasma potential near the location of the collection probe without appreciable perturbation to the plasma. The lowest temperatures are obtained when the floating electrode is combined with RF chokes that increase the circuit impedance. This design can be used in any RF discharge, even one with strong magnetic fields. We have also shown that the second harmonic generated in the probe sheath or in the helicon discharge needs to be annulled in order to obtain accurate temperature measurements, and that the conductivity of the probe shaft is immaterial if the RF compensation is strong enough.

Acknowledgments

We are grateful to Dr Gaétan Chevalier, who participated in the measurements. This work was partially supported by the University of Wisconsin's Engineering Center for Plasma-Aided Manufacturing.

References

[1] Boswell R W 1984 *Plasma Phys. Control. Fusion* **26** 1147
[2] Chen F 1992 *J. Vac. Sci. Technol.* A **10** 1389
[3] Perry A J and Boswell R W 1989 *Appl. Phys. Lett.* **55** 148
Charles C 1993 *J. Vac. Sci. Technol.* A **11** 157
[4] Kitagawa H, Tsunoda A, Shindo H and Horiike Y 1993 *Plasma Sources Sci. Technol.* **2** 11
Jiwari N, Iwasawa H, Narai A, Sakaue H, Shindo H, Shoji T and Horiike Y 1993 *Japan. J. Appl. Phys.* **32** 3019
[5] Garscadden A and Emelus K G 1962 *Proc. Phys. Soc.* **79** 535
[6] Boschi A and Magistrelli F 1963 *Nuovo Cimento* **29** 487
[7] Chen F F 1964 *Rev. Sci. Instrum.* **35** 1208
[8] Cantin A and Gagne R R J 1977 *Appl. Phys. Lett.* **30** 316
[9] Braithwaite N St J, Benjamin N M P and Allen J E 1987 *J. Phys. E: Sci. Instrum.* **20** 1046
[10] Paranjpe A P, McVittie J P and Self S A 1990 *J. Appl. Phys.* **67** 6718
[11] Lai C, Breun R A, Sandstrom P W, Wendt A E, Hershkowitz N and Woods R C 1993 *J. Vac. Sci. Technol.* A **11** 1199
[12] Godyak V A, Piejak R B and Alexandrovich B M 1992 *Plasma Sources Sci. Technol.* **1** 36
[13] Bills D G, Holt R B and McClure B T 1992 *J. Appl. Phys.* **33** 29
[14] Sanmartin J 1970 *Phys. Fluids* **13** 103
[15] Stangeby P C 1982 *J. Phys. D: Appl. Phys.* **15** 1007
[16] Chen F F 1965 *J. Appl. Phys.* **36** 675